Supplementary Information (SI) for

Strong compensation effects related to the empty channel in p-type transparent conductive material Cu_3TaS_4: a first-principles study

Yang Xue,[a] Zhihao Zhuo,[b,c] Changqing Lin,[a] Dan Huang*[a,c]

a. Guangxi Novel Battery Materials Research Center of Engineering Technology, State Key Laboratory of Featured Metal Materials and Life-cycle Safety for Composite Structures, School of Physical Science and Technology Guangxi University, Nanning 530004, China. E-mail: danhuang@gxu.edu.cn.
b. Guangxi Institute of Scientific and Technical Information, Nanning 530021, China.
c. Guangxi Key Laboratory of Precision Navigation Technology and Application, Guilin University of Electronic Technology, Guilin 541004, China;

Corresponding Authors:

*E-mail danhuang@gxu.edu.cn. (Dan Huang)

The calculation details of optical properties

To calculate the optical properties, it is essential to obtain the dielectric function $\varepsilon\,(\omega)$ of material. In general, the dielectric function is divided as two part: $\varepsilon\,(\omega) = \varepsilon_1(\omega) + i\varepsilon_2(\omega)$, in which $\varepsilon_1(\omega)$ and $\varepsilon_2(\omega)$ are real part of dielectric function and imaginary part of dielectric function, respectively [1-2].

For the imaginary part of dielectric function, it can be given as the following [3]:

$$\varepsilon_2(\omega) = \frac{Ve^2}{2\pi\hbar m^2\omega^2}\int d^3k \sum_{nn'} |<kn|p|kn'>|^2 f(kn) \times \left[1 - f(kn')\right]\delta\left(E_{kn} - E_{kn'} - \hbar\omega\right). (1)$$

In the equation (1), $\hbar\omega$ denotes the energy of the incident photon, while p represents the momentum operator. The eigenfunction corresponding to the eigenvalue E_{kn} is denoted by $|kn>$, and $f(kn)$ signifies the Fermi distribution function.

Based on the imaginary part of dielectric function, the real part of dielectric function is calculated by integrating the obtained imaginary part with the Kramers-Kronig relation [4]:

$$\varepsilon_1(\omega) = 1 + \frac{2}{\pi}P\int_0^\infty \frac{\omega'\varepsilon_2(\omega')}{\omega'^2 - \omega^2}d\omega'.\#(2)$$

Here, P is the principal value of the integral, ω is the frequency.

After obtain the real part of dielectric function and the imaginary part of dielectric function, the optical parameters such as absorption coefficient $\alpha(\omega)$, reflectivity $R(\omega)$, optical conductivity [$\sigma(\omega)$] can be calculated based on the following [5-7]:

$$\alpha(\omega) = \frac{\omega}{c}\sqrt{2\left(\sqrt{\varepsilon_1^2(\omega) + \varepsilon_2^2(\omega)} - \varepsilon_1(\omega)\right)}, \#(3)$$

$$R(\omega) = \left|\frac{\sqrt{\varepsilon_1(\omega) + \varepsilon_2(\omega)} - 1}{\sqrt{\varepsilon_1(\omega) + i\varepsilon_2(\omega)} + 1}\right|^2, \#(4)$$

$$\sigma(\omega) = \frac{\omega}{4\pi}\varepsilon_2(\omega). \# (5)$$

The growth and quenching processes

The growth temperature in theoretical simulations should be precisely matched with experimental conditions to ensure a meaningful comparison. In the experimental work regarding the preparation of Cu_3TaS_4, various crystal growth processes have been reported. The temperatures typically involved in these processes range from 780 °C (1053 K) [8] to 850 °C (1123 K) [9]. To ensure structural stability in the calculations while maintaining consistency with experimental conditions, we set an upper temperature limit of 1200 K. This threshold not only accommodates the highest reported experimental growth temperature but also provides sufficient structural stability for reliable computational analysis.

During the quenching process, the sample should be rapidly cooled to room temperature (*i.e.* 300 K) to preserve the total defect concentration generated during high-temperature synthesis.

In our calculations, the growth and quenching processes can be calculated based on the following equations:

$$n(\alpha^0) = N_\alpha^{GT} \frac{g_q e^{-\frac{\Delta H_f(\alpha,0)}{K_B Q T}}}{g_q e^{-\frac{\Delta H_f(\alpha,0)}{K_B Q T}} + g_q e^{-\frac{\Delta H_f(\alpha,q)}{K_B Q T}}}, \#(6)$$

$$n(\alpha^q) = N_\alpha^{GT} \frac{g_q e^{-\frac{\Delta H_f(\alpha,q)}{K_B QT}}}{g_q e^{-\frac{\Delta H_f(\alpha,0)}{K_B QT}} + g_q e^{-\frac{\Delta H_f(\alpha,q)}{K_B QT}}}. \#(7)$$

Equation (6) represents the defect concentration with the charge state 0, in which N_α^{GT} is the total number of defects α. g_q is the degeneracy factor related to possible electron configurations. K_B is the Boltzmann constant, $\Delta H_f(\alpha,0)$ is the defect formation energy corresponding defect $\alpha$with the charge state 0. GT and QT are growth temperature and quenching temperature, respectively. Equation (7) represents the defect concentration with the charge state q.

The estimation of the electron concentration

Based on the principle of detailed balance, the system needs to satisfy the charge neutrality condition:

$$n + N_A^- = p + N_D^+ \#(8)$$

where *n* (and *p*) represents the density of the excited electrons (and holes) that are generated from the total concentration of the ionized acceptors N_A^- (and donors N_D^+).

At a certain temperature, these carrier densities *n* and *p* depend on the Fermi level E_F

$$\begin{gathered} n = N_c e^{-\frac{E_c - E_F}{k_B T}}, N_c = 2\frac{\left(2\pi m_n^* k_B T\right)^{\frac{3}{2}}}{h^3} \\ p = N_v e^{-\frac{E_F - E_v}{k_B T}}, N_v = 2\frac{\left(2\pi m_p^* k_B T\right)^{\frac{3}{2}}}{h^3}, \end{gathered} \#(9)$$

where N_c and N_v are the effective density states of the conduction and valence bands, respectively. m_n^* and m_p^* stands for the electron and hole effective masses, respectively.

According to the equation (9), the total carrier concentration is calculated as the following:

$$n_i^{\;2} = np = N_C N_v e^{-\frac{E_c - E_v}{k_B T}} = N_C N_v e^{-\frac{E_g}{k_B T}}.\#(10)$$

Based on the calculated results, the hole concentration of intrinsic Cu_3TaS_4 under Cu-poor conduction is estimated to 1.00×10^{15} cm^{-3}. Therefore, the electron concentration is estimated to 1.04×10^{5} cm^{-3}.

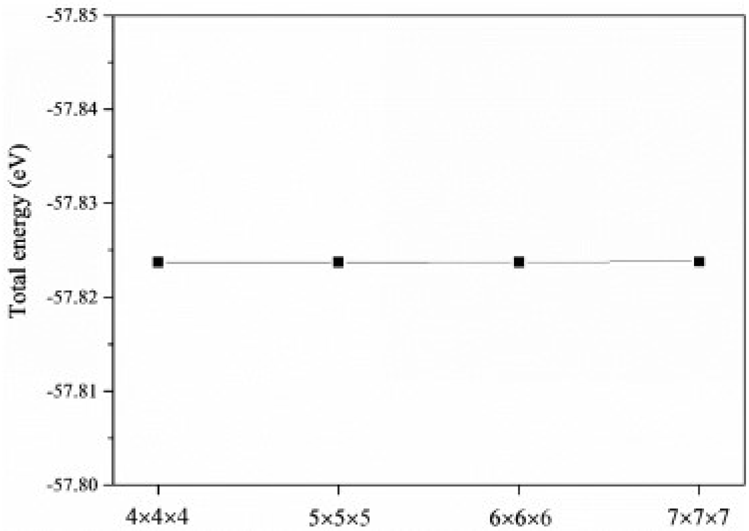

Fig. S1. The calculated total energies of Cu_3TaS_4 unit cell using different K-meshes.

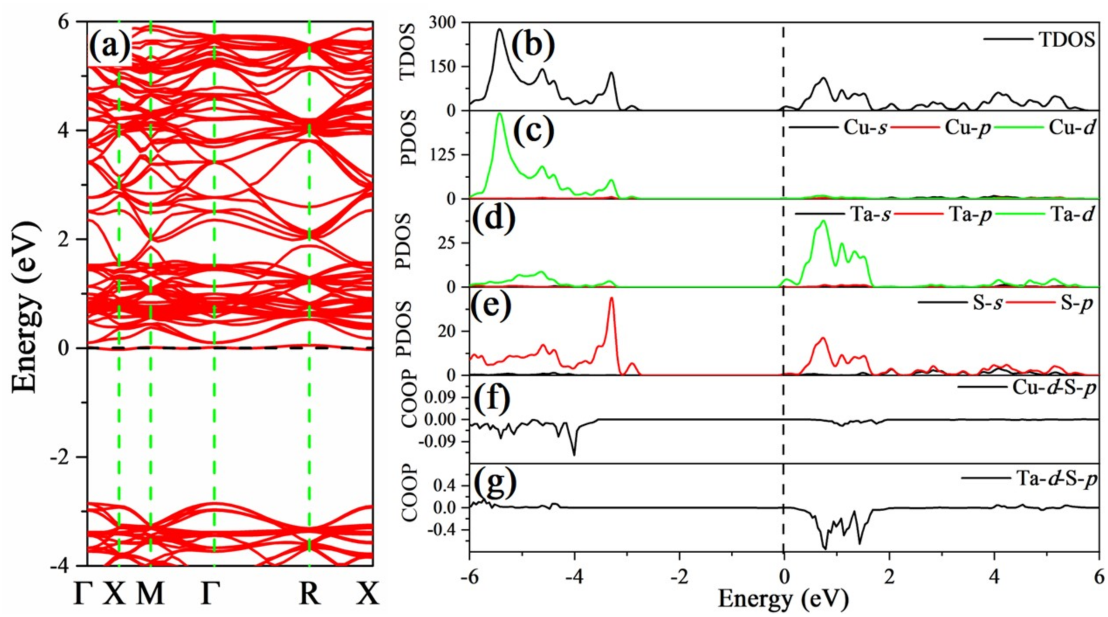

Fig. S2. The band structure (a) and the TDOS (b), PDOSs (c-e) as well as the COOPs (f-g) after the introduction of the Cu_i into the Cu_3TaS_4. The black horizontal and vertical dotted lines represent the Fermi level.

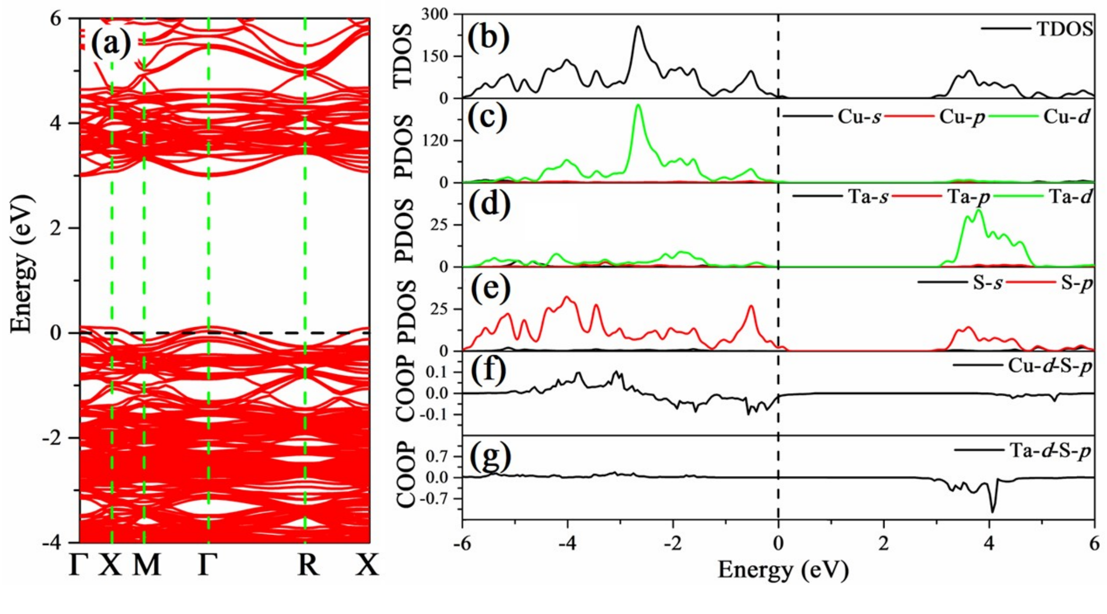

Fig. S3. The band structure (a) and the TDOS (b), PDOSs (c-e) as well as the COOPs (f-g) after the introduction of the V_{Cu} into the Cu_3TaS_4. The black horizontal and vertical dotted lines represent the Fermi level.

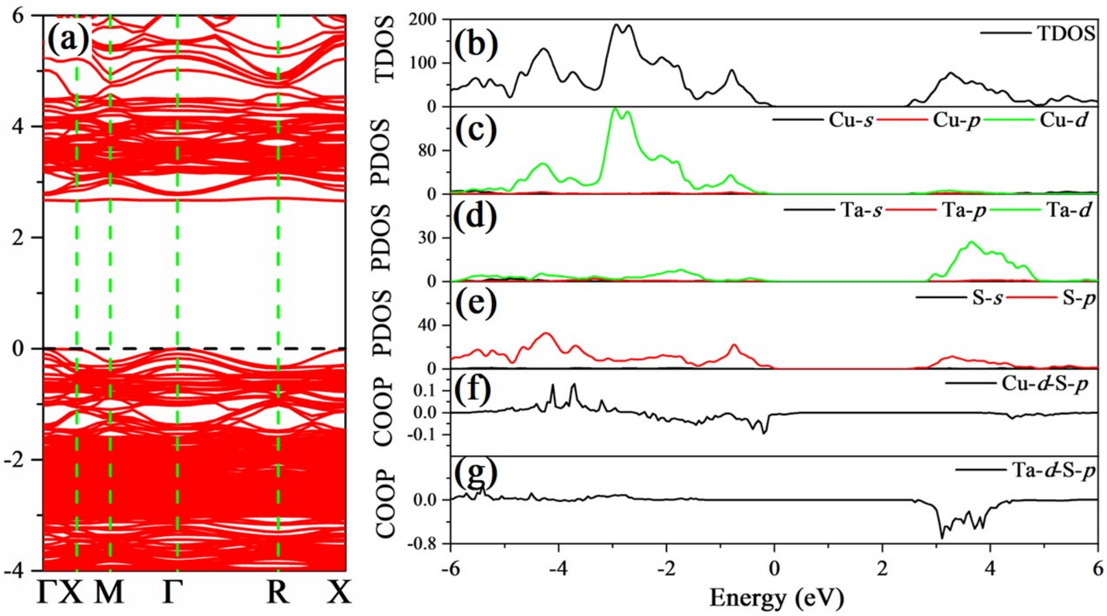

Fig. S4. The band structure (a) and the TDOS (b), PDOSs (c-e) as well as the COOPs (f-g) after the introduction of the defect complex V_{Cu}+Cu_i into the Cu_3TaS_4. The black horizontal dotted line represents the Fermi level.

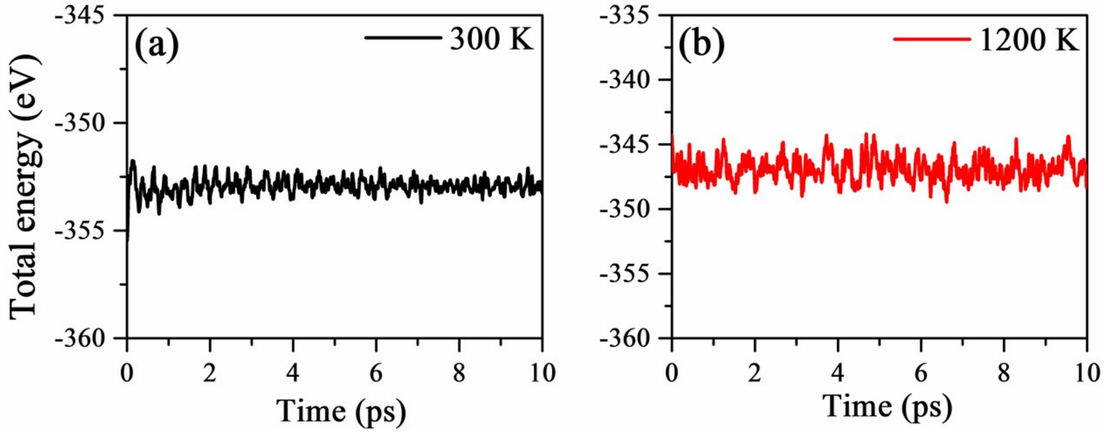

Fig. S5. The molecular dynamics simulations at 300 K (a) and 1200 K (b) within 10 ps.

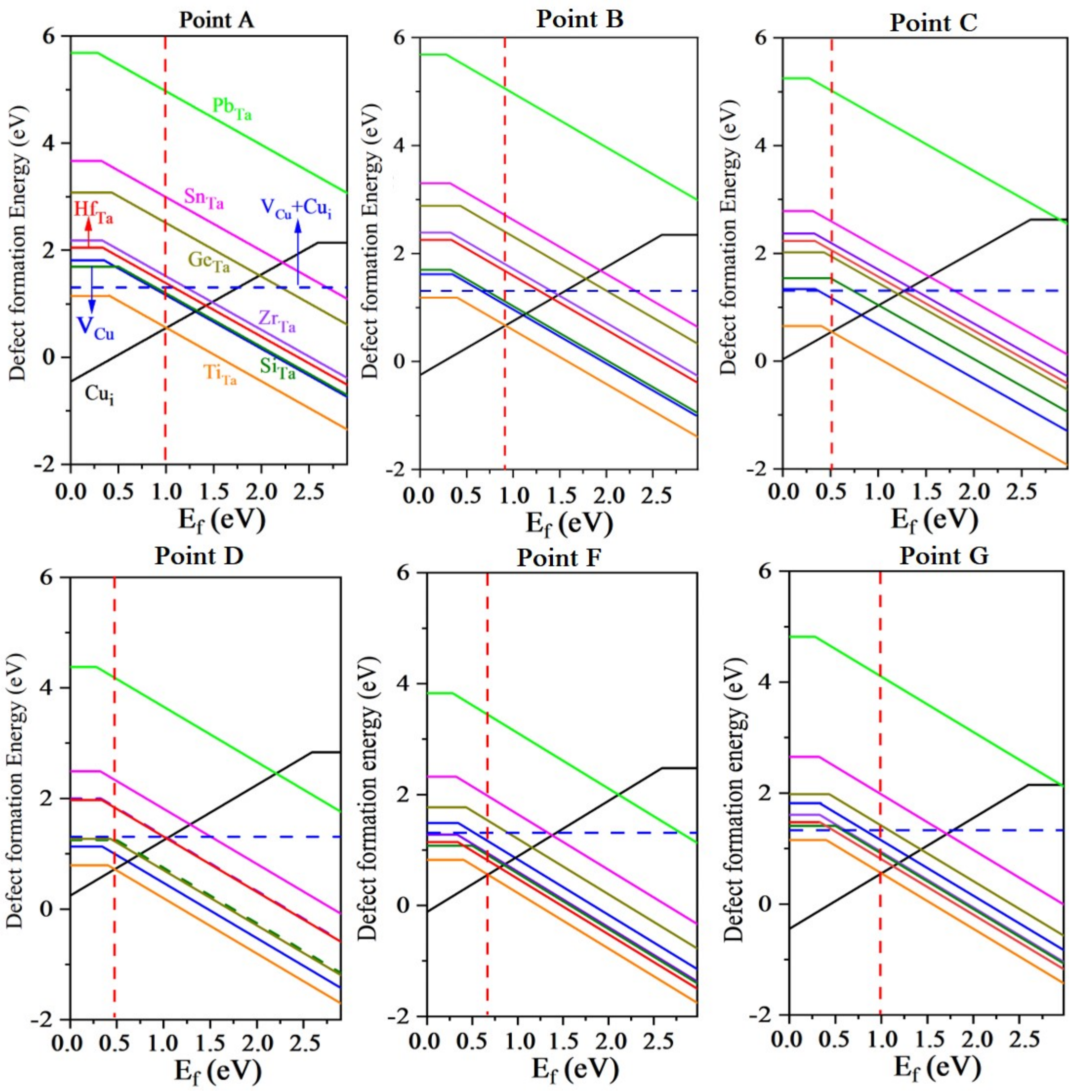

Fig. S6. The defect formation energies of p-type doping at Ta site as a function of Fermi level under six remaining chemical potential environments (point A to point D and point F to point G), respectively. The red vertical dotted line is the Fermi level at 300 K.

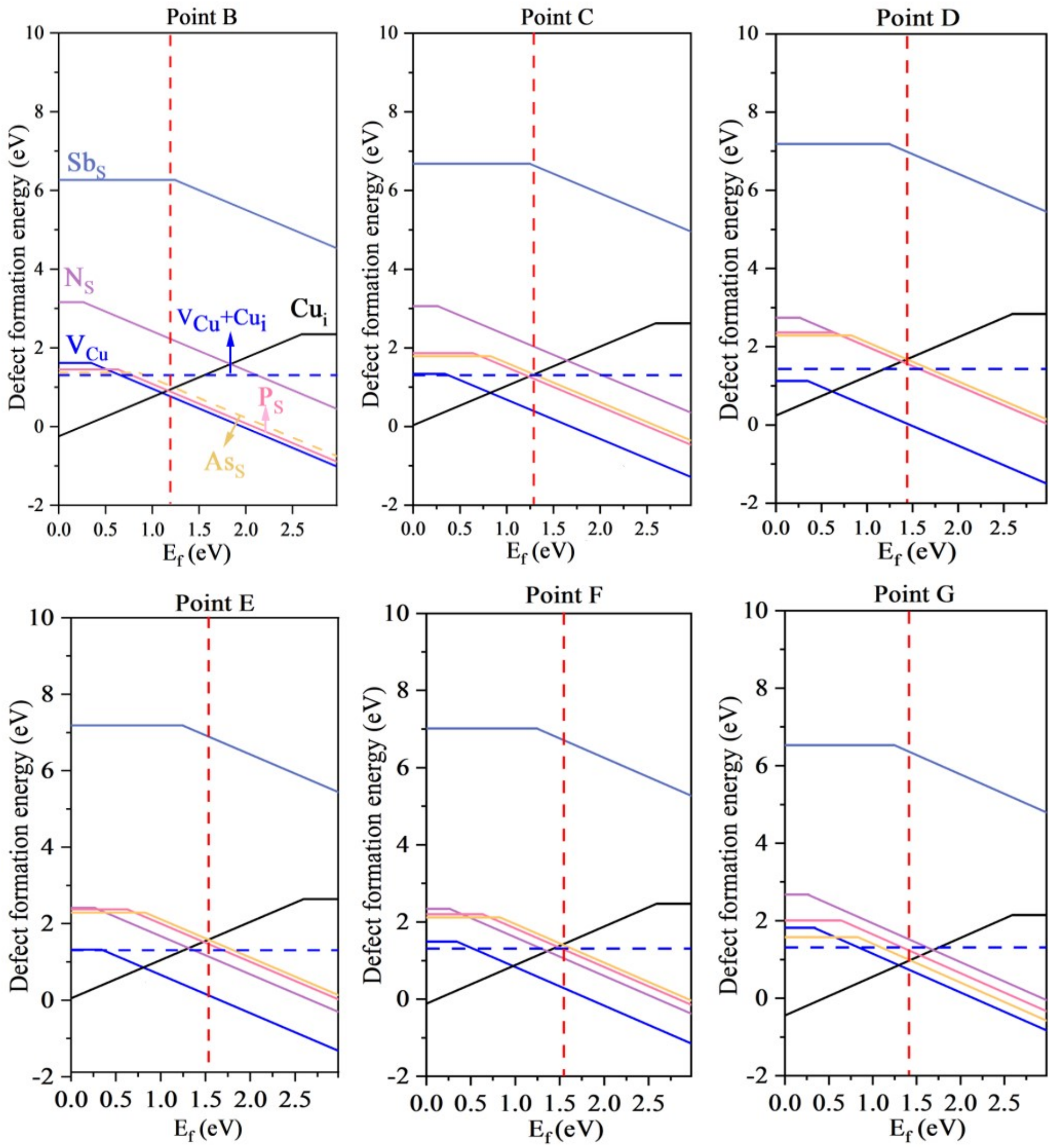

Fig. S7. The defect formation energies of p-type doping at S site as a function of Fermi level under six remaining chemical potential environments (point B to point G), respectively. The red vertical dotted line is the Fermi level at 300 K.

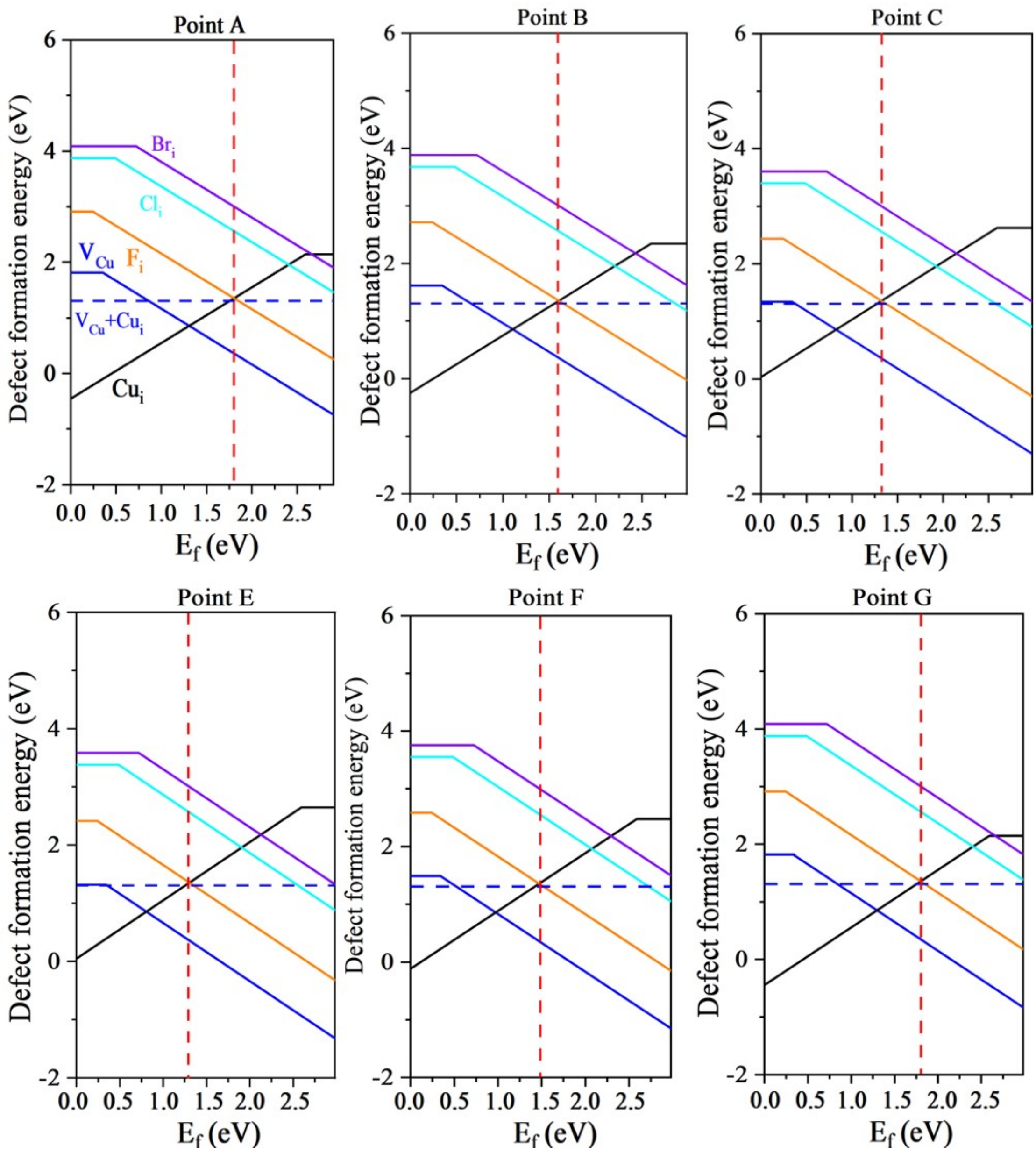

Fig. S8. The defect formation energies of interstitial defects at points A-C and points E-G as a function of Fermi level. The red vertical dotted line is the Fermi level at 300 K.

Table S1. The carrier mobility, bipolar Seebeck coefficient of pristine Cu_3TaS_4 at 300 K and the effective masses along different directions.

Conductivity type	Carrier concentration (cm^{-3})	Carrier mobility (cm^2/Vs)	Seebeck coefficient (μV/K)	Effective mass (m_e)	
n	1.04×10^{5}	39.30	-2820	X-Γ	3.86
				X-R	0.94
				X-M	0.94
p	1.00×10^{15}	43.10	1150	R-X	1.23
				R-Γ	1.02
				R-M	3.35

To assess the relative chemical potentials of the dopants, a series of competing compounds are considered as the following:

$$2\Delta\mu_{Cu} + \Delta\mu_{Si} + 3\Delta\mu_S \leq \Delta H(Cu_2SiS_3) =- 3.44eV\#(11)$$

$$4\Delta\mu_{Cu} + \Delta\mu_{Ge} + 4\Delta\mu_S \leq \Delta H(Cu_4GeS_4) =- 3.38eV\#(12)$$

$$2\Delta\mu_{Cu} + \Delta\mu_{Sn} + 3\Delta\mu_S \leq \Delta H(Cu_2SnS_3) =- 2.63eV\#(13)$$

$$\Delta\mu_{Pb} + \Delta\mu_S \leq \Delta H(PbS) =- 1.14eV\#(14)$$

$$4\Delta\mu_{Cu} + \Delta\mu_{Ti} + 4\Delta\mu_S \leq \Delta H(Cu_4TiS_4) =- 6.67eV\#(15)$$

$$\Delta\mu_{Zr} + 2\Delta\mu_S \leq \Delta H(ZrS_2) =- 5.02eV\#(16)$$

$$\Delta\mu_{Hf} + 3\Delta\mu_S \leq \Delta H(HfS_3) =- 5.29eV\#(17)$$

$$3\Delta\mu_{Ta} + 5\Delta\mu_N \leq \Delta H(Ta_3N_5) =- 3.44eV\#(18)$$

$$3\Delta\mu_{Cu} + \Delta\mu_P \leq \Delta H(Cu_3P) =- 0.47eV\#(19)$$

$$3\Delta\mu_{Cu} + \Delta\mu_{As} \leq \Delta H(Cu_3As) =- 0.13eV\#(20)$$

$$3\Delta\mu_{Cu} + \Delta\mu_{Sb} \leq \Delta H(Cu_3Sb) =- 0.12eV\#(21)$$

$$\Delta\mu_{Cu} + \Delta\mu_F \leq \Delta H(CuF) =- 2.10eV\#(22)$$

$\Delta\mu_{Cu} + \Delta\mu_{Cl} \leq \Delta H(CuCl) =- 1.29eV\#(23)$

$\Delta\mu_{Cu} + \Delta\mu_{Br} \leq \Delta H(CuBr) =- 1.05eV\#(24)$

References:

[1] M. Barhoumi, N. Sfina, S. Znaidia, First-principles calculations of optical properties of 2D CaFBr and BaFBr monolayers, Physica E, 137 (2022) 115074.

[2] Y. Al-Douri, M. Ameri, A. Bouhemadou, K. M. Batoo, First-principles calculations to investigate the refractive index and optical dielectric constant of Na_3SbX_4 (X= S, Se) ternary chalcogenides, Phys. Status Solidi B, 256(11) (2019) 1900131.

[3] A. Bekhti-Siad, K. Bettine, D. P. Rai, Y. Al-Douri, X. Wang, R. Khenata, A. Bouhemadou, C. H. Voon, Electronic, optical and thermoelectric investigations of Zintl phase AE_3AlAs_3 (AE=Sr, Ba): first-principles calculations, Chinese J. Phys., 56(3) (2018) 870-879.

[4] H. R. Philipp, H. Ehrenreich, Optical properties of semiconductors, Phys. Rev., 129(4) (1963) 1550.

[5] S. Zhang, X. Zhang, Y. Zhu, S. Zhang, L. Qi, R. Liu, First-principles investigations on elastic and thermodynamic properties of zirconium under pressure, Comput. Mater. Sci., 61 (2012) 42-49.

[6] Z. Souadia, A. Bouhemadou, R. Khenata, Y. Al-Douri, Structural, elastic and lattice dynamical properties of the alkali metal tellurides: First-principles study, Physica B, 521 (2017) 204-214.

[7] R. Chen, D. Chen, W. Zhang, First-principles calculations to investigate stability, electronic and optical properties of fluorinated $MoSi_2N_4$ monolayer, Results Phys., 30 (2021) 104864.

[8] P. F. Newhouse, P. A. Hersh, A. Zakutayev, A. Richard, H. A. S. Platt, D. A. Keszler and J. Tate, Thin film preparation and characterization of wide band gap Cu_3TaQ_4 (Q = S or Se) p-type semiconductors, Thin Solid Films, 2009, 517, 2473–2476.

[9] G. E. Delgado, J. E. Contreras, A. J. Mora, S. Durán, M. Muñoz and P. Grima-Gallardo, Structure Refinement of the Semiconducting Compound Cu_3TaS_4 from X-

Ray Powder Diffraction Data, Acta Phys. Pol. A, 2011, 120, 468–472.